Early sarcomere and metabolic defects in a zebrafish *pitx2c* cardiac arrhythmia model

Michelle M. Collins[a,b,1], Gustav Ahlberg[c,d], Camilla Vestergaard Hansen[e], Stefan Guenther[f], Rubén Marín-Juez[a,b], Anna M. Sokol[a,b,g], Hadil El-Sammak[a], Janett Piesker[h], Ylva Hellsten[e], Morten S. Olesen[c,d], Didier Y. R. Stainier[a,b,1], and Pia R. Lundegaard[c,d,1]

[a]Department of Developmental Genetics, Max Planck Institute for Heart and Lung Research, D-61231 Bad Nauheim, Germany; [b]DZHK German Centre for Cardiovascular Research, Partner Site Rhine-Main, D-61231 Bad Nauheim, Germany; [c]Laboratory for Molecular Cardiology, Department of Cardiology, Vascular, Pulmonary and Infectious Diseases, University Hospital of Copenhagen, 2100 Copenhagen, Denmark; [d]Department of Biomedical Sciences, University of Copenhagen, 2200 Copenhagen, Denmark; [e]Department of Nutrition, Exercise and Sport, University of Copenhagen, 2200 Copenhagen, Denmark; [f]Bioinformatics and Deep Sequencing Platform, Max Planck Institute for Heart and Lung Research, D-61231 Bad Nauheim, Germany; [g]Biomolecular Mass Spectrometry, Max Planck Institute for Heart and Lung Research, D-61231 Bad Nauheim, Germany; and [h]Microscopy Service Group, Max Planck Institute for Heart and Lung Research, D-61231 Bad Nauheim, Germany

Edited by Calum A. MacRae, Harvard Medical School, Boston, MA, and accepted by Editorial Board Member Christine E. Seidman October 2, 2019 (received for review August 12, 2019)

Atrial fibrillation (AF) is the most common type of cardiac arrhythmia. The major AF susceptibility locus 4q25 establishes long-range interactions with the promoter of *PITX2*, a transcription factor gene with critical functions during cardiac development. While many AF-linked loci have been identified in genome-wide association studies, mechanistic understanding into how genetic variants, including those at the 4q25 locus, increase vulnerability to AF is mostly lacking. Here, we show that loss of *pitx2c* in zebrafish leads to adult cardiac phenotypes with substantial similarities to pathologies observed in AF patients, including arrhythmia, atrial conduction defects, sarcomere disassembly, and altered cardiac metabolism. These phenotypes are also observed in a subset of *pitx2c*$^{+/-}$ fish, mimicking the situation in humans. Most notably, the onset of these phenotypes occurs at an early developmental stage. Detailed analyses of *pitx2c* loss- and gain-of-function embryonic hearts reveal changes in sarcomeric and metabolic gene expression and function that precede the onset of cardiac arrhythmia first observed at larval stages. We further find that antioxidant treatment of *pitx2c*$^{-/-}$ larvae significantly reduces the incidence and severity of cardiac arrhythmia, suggesting that metabolic dysfunction is an important driver of conduction defects. We propose that these early sarcomere and metabolic defects alter cardiac function and contribute to the electrical instability and structural remodeling observed in adult fish. Overall, these data provide insight into the mechanisms underlying the development and pathophysiology of some cardiac arrhythmias and importantly, increase our understanding of how developmental perturbations can predispose to functional defects in the adult heart.

cardiac development | cardiomyopathy | cardiac metabolism | transcriptional profiling

The most prevalent defect affecting cardiac conduction is atrial fibrillation (AF), a common sustained arrhythmia associated with increased risk of cardioembolic stroke or sudden death. Despite its clinical importance, mechanisms underlying the initiation and pathogenesis of AF remain poorly understood. The genetic component of AF has been investigated through large-scale genome-wide association studies. The most prominently associated region is 4q25, an intergenic region with at least four independent AF association loci in close proximity to the *PITX2* gene (1–4). A role for PITX2 in AF pathogenesis has been demonstrated by animal model studies (5–10). More recently, chromosome conformation capture (3C) studies have shown that 4q25 interacts with the promoter of the cardiac-specific isoform of *PITX2C*, further supporting the hypothesis that 4q25 variants regulate *PITX2C* expression (11).

PITX2 is a transcription factor that plays critical roles during cardiac morphogenesis. Three isoforms are generated from two promoters and alternative splicing. *PITX2C* is the major isoform expressed in the heart, with enrichment in the left atrium. It has previously been observed that *PITX2* messenger RNA (mRNA) levels are reduced in the atrial cardiomyocytes (CMs) of sustained AF patients carrying risk variants at 4q25 (12). Additionally, *PITX2* gain-of-function variants have also been associated with AF in humans, suggesting that expression levels of PITX2 targets must be tightly regulated for cardiac homeostasis (13, 14). During vertebrate development, Pitx2 is a key regulator of left–right patterning of the body plan (15–17). Within the conduction system, Pitx2 seems to play a similar role to repress left-sided pacemaker identity (5, 7, 9). Adult *Pitx2*$^{+/-}$ mice are prone to AF when paced, likely as a developmental patterning defect arising from expanded pacemaker gene expression (5, 7). Conditional genetic mouse models reveal a postnatal function for Pitx2 in directly regulating genes encoding

Significance

Atrial fibrillation (AF) is the most common cardiac arrhythmia, affecting 2 to 3% of the general population and leading to significant morbidity and mortality. Genome-wide association studies identified the 4q25 AF risk locus, a region that forms long-range interactions with the promoter of *PITX2*, which encodes a critical transcriptional regulator of cardiac development. Using a zebrafish *pitx2c* loss-of-function model, we find that larval and adult zebrafish phenocopy many hallmarks of human AF. Our data further indicate that the pathogenesis of arrhythmia and AF-like phenotypes in *pitx2c* mutants is driven by developmental perturbations to sarcomere organization and metabolic pathways. We also find that antioxidant treatment reduces the incidence and severity of cardiac arrhythmia, suggesting avenues for therapeutic strategies.

Author contributions: M.M.C., M.S.O., D.Y.R.S., and P.R.L. designed research; M.M.C., C.V.H., S.G., J.P., Y.H., and P.R.L. performed research; R.M.-J., A.M.S., and H.E.-S. contributed new reagents/analytic tools; M.M.C., G.A., C.V.H., S.G., M.S.O., D.Y.R.S., and P.R.L. analyzed data; and M.M.C., D.Y.R.S., and P.R.L. wrote the paper.

The authors declare no competing interest.

This article is a PNAS Direct Submission. C.A.M. is a guest editor invited by the Editorial Board.

Data deposition: The data reported in this paper have been deposited in the Gene Expression Omnibus (GEO) database, https://www.ncbi.nlm.nih.gov/geo (accession no. GSE128511).

[1]To whom correspondence may be addressed. Email: michelle.collins@mpi-bn.mpg.de, didier.stainier@mpi-bn.mpg.de, or plundegaard@sund.ku.dk.

This article contains supporting information online at www.pnas.org/lookup/suppl/doi:10.1073/pnas.1913905116/-/DCSupplemental.

First published November 8, 2019.

ion channels and cell–cell junctions, thereby affecting cardiac action potentials (18).

Mechanisms of AF initiation and pathogenesis are not well understood. Developmental defects have been proposed to predispose to AF as indicated by association with developmental genes, such as *PITX2*. These defects are thought to result in subclinical abnormalities in the adult heart that can subsequently manifest as AF after induction by aging, disease, or stress. Additionally, mutations in genes required to maintain CM structure, such as titin-truncating variants and lesions in the atrial-specific myosin light chain gene *MYL4*, have been shown to predispose to AF (19–21), indicating that the disease is not only caused by electrical disturbances.

Here, we show that *pitx2c*$^{-/-}$ adult zebrafish display many pathologies found in human AF patients, including atrial conduction defects, general structural remodeling, and altered cardiac metabolism. Using transcriptomics approaches, we find that Pitx2c is a critical regulator of sarcomeric and metabolic gene expression during embryogenesis. Notably, we show that treatment with the antioxidant *N*-acetyl cysteine (NAC) can rescue cardiac arrhythmia in *pitx2c*$^{-/-}$ larvae, suggesting that altered mitochondrial-derived oxidative stress is an important driver of arrhythmia in conjunction with abnormal sarcomere organization. These data indicate that developmental perturbations to sarcomere function and metabolic pathways contribute to arrhythmia and AF-like pathologies.

Results

Loss of Pitx2c Leads to Altered Cardiac Function and Cardiomyopathy in Adult Zebrafish. We investigated a recently generated loss-of-function allele of *pitx2c* (*pitx2c*^{ups6}) in zebrafish (22) and assessed its adult cardiac phenotype. *pitx2c*$^{ups6/up6}$ (hereafter referred to as *pitx2c*$^{-/-}$) are fertile and survive until adulthood; however, increased mortality rates are observed compared with *pitx2c*$^{+/+}$ siblings (*SI Appendix*, Fig. S1*A*). To evaluate whether cardiac function was affected, we first performed echocardiography on adult fish (Fig. 1 *A*–*E*). We quantified parameters of cardiac function by Brightfield-Mode (B-Mode) imaging as well as pulsed-wave Doppler imaging of blood flow. B-Mode imaging of

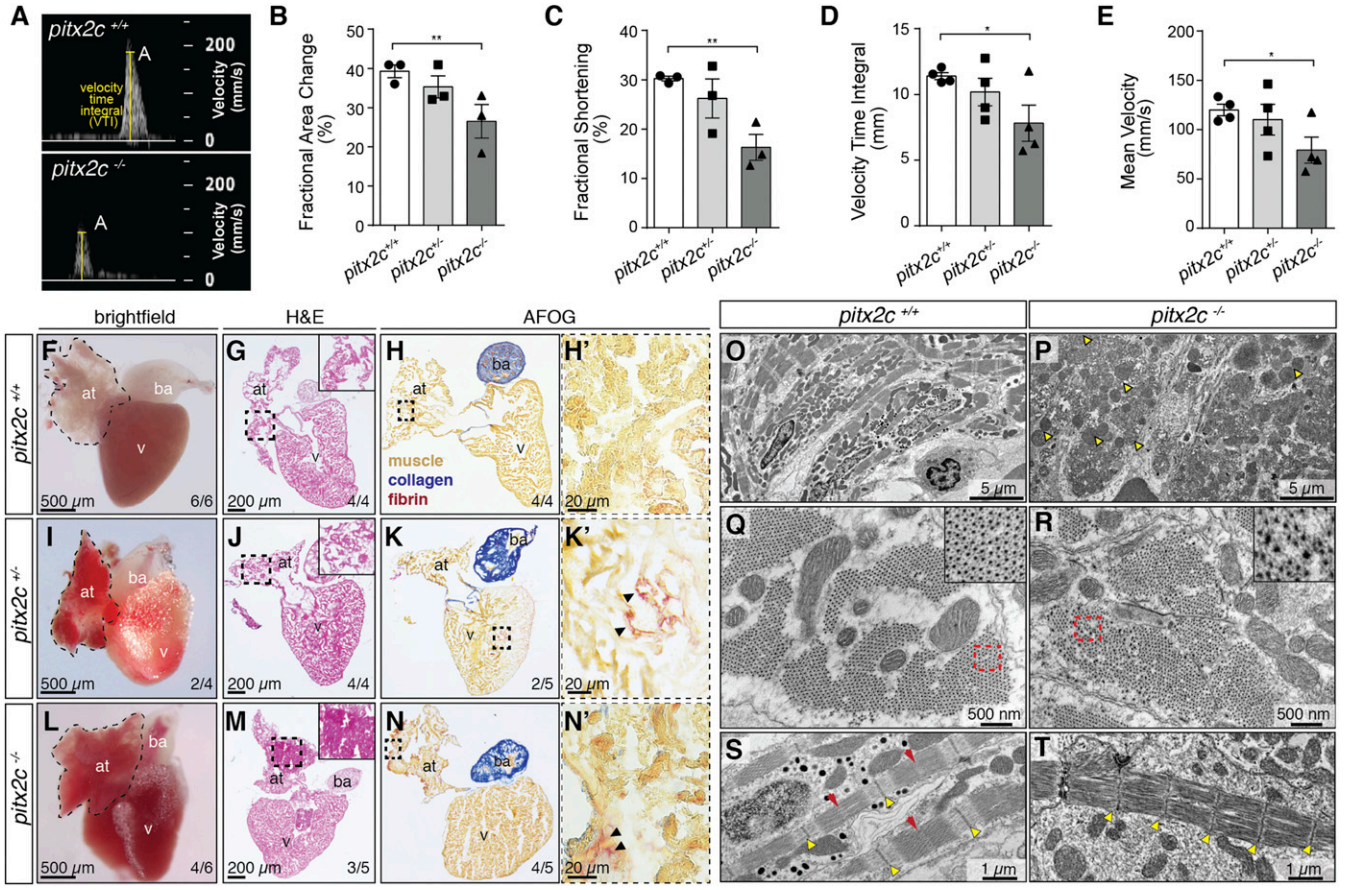

Fig. 1. Loss of Pitx2c disrupts cardiac function and structure in adult zebrafish. (*A*–*E*) Analysis of cardiac function by echocardiography. Brightfield-Mode (B-Mode) imaging of long-axis views was used to quantify FAC and FS. Pulsed-wave Doppler imaging (*A*) was used to quantify peak A VTI and mean blood flow velocity (*E*). Individual data points represent an average measurement taken from 3 diastolic/systolic phases of each fish. All parameters of cardiac function are significantly reduced in *pitx2c*$^{-/-}$ adults, with variability observed in *pitx2c*$^{+/-}$ siblings. (*F*–*N*) Adult cardiac morphology at 14 months postfertilization (mpf). Dashed lines outline the atrium in whole-mount view of hearts (*F*, *I*, and *L*). Histology was analyzed by hematoxylin and eosin (H&E) staining (*G*, *J*, and *M*; *Insets* show higher magnification of the boxed region), and fibrosis was analyzed by Acid Fuchsin Orange G (AFOG) staining (*H*, *K*, and *N*; higher magnification of the boxed regions are shown in *H*′, *K*′, and *N*′). *pitx2c*$^{-/-}$ hearts display enlarged and blood-filled atria (*L*), and atrial tissue appears hypertrophic (*M*, *Inset*). Fibrotic foci are present in the atrium of *pitx2c*$^{-/-}$ fish (*N*′; black arrowheads). Intermediate phenotypes were observed in *pitx2c*$^{+/-}$ hearts. at, atrium; ba, bulbus arteriosus; v, ventricle. (*O*–*T*) TEM images of adult *pitx2c*$^{+/+}$ and *pitx2c*$^{-/-}$ atria ($n = 3$). Areas of highly damaged and necrotic tissue are observed in *pitx2c*$^{-/-}$ atria, with an increased number of mitochondria that appear enlarged and defective (*P*; yellow arrowheads). Representative images of cross-sections through myofibril bundles (*Q* and *R*; *Q*, *Inset* and *R*, *Inset* show higher magnifications) and longitudinal sections of sarcomeres (*S* and *T*). *pitx2c*$^{-/-}$ atria exhibit disorganized myofibril bundles and poorly defined Z discs (yellow arrowheads), and M lines (red arrows) are difficult to distinguish (*T*). Error bars indicate SEM. **P* < 0.05 by unpaired *t* test; ***P* < 0.01 by unpaired *t* test.

sagittal long-axis views revealed cardiac dysfunction in *pitx2c*$^{-/-}$ compared with *pitx2c*$^{+/+}$ siblings (Movies S1 and S2). From these views, we measured ventricular area and length during systole and diastole to quantify fractional area change (FAC) and fractional shortening (FS), respectively. *pitx2c*$^{-/-}$ adults exhibit significantly reduced FAC and FS (26.5 ± 0.043%; 16.3 ± 0.026%, respectively) compared with *pitx2c*$^{+/+}$ siblings (39.3 ± 0.016%, P = 0.0495; 30.3 ± 0.005%, P = 0.0065). Quantification of peak ejection blood flow parameters (Fig. 1*A*) revealed a reduction in ventricular velocity time integral (VTI) (Fig. 1*D*) and mean ventricular velocity (Fig. 1*E*) in *pitx2c*$^{-/-}$ (11.4 ± 0.26 mm; 120.0 ± 5.8 mm/s, respectively) compared with *pitx2c*$^{+/+}$ siblings (7.8 ± 1.4 mm, P = 0.0428; 79.17 ± 13.2 mm/s, P = 0.0296). Together, these data indicate impaired cardiac function in *pitx2c*$^{-/-}$ adult zebrafish.

We next analyzed gross cardiac morphology. On dissection of adult hearts, we found that a subset of *pitx2c*$^{-/-}$ atria was enlarged and remained filled with blood following perfusion with saline (Fig. 1*L*). Subsequent histological analysis of *pitx2c*$^{-/-}$ atria revealed hypertrophic regions (Fig. 1*M*) as well as focal areas of collagen and fibrin staining, suggesting increased fibrosis (Fig. 1 *N* and *N*′). To confirm the presence of fibrosis, we measured mRNA levels of the profibrotic genes *acta2* and *col1a1a* by qPCR and observed their up-regulation in *pitx2c*$^{-/-}$ hearts compared with *pitx2c*$^{+/+}$ (*SI Appendix*, Fig. S1*B*). We noted similar phenotypes in a subset of *pitx2c*$^{+/-}$ adults (~50%) (Fig. 1 *I*–*K*). We did not detect obvious fibrosis in young adult hearts (*SI Appendix*, Fig. S1 *C*–*H*), suggesting that fibrosis likely arises as a secondary consequence of altered cardiac function.

To examine cardiac morphology at the ultrastructural level, we performed transmission electron microscopy (TEM) on atria of *pitx2c*$^{+/+}$ and *pitx2c*$^{-/-}$ adult fish (Fig. 1 *O*–*T*). Atrial tissue architecture in *pitx2c*$^{-/-}$ was heterogenous, with extensive areas of necrosis and tissue damage (Fig. 1*P*). Mitochondrial morphology was also variable, with many smaller dilated mitochondria observed in *pitx2c*$^{-/-}$ atria (Fig. 1*P*). Cross-sections through sarcomeres in *pitx2c*$^{+/+}$ atria revealed parallel arrangement of thick and thin filaments forming a tight hexagonal array (Fig. 1*Q*), with clearly defined Z discs and M lines that anchor myofibrils in place (Fig. 1*S*). In contrast, myofibrils were disorganized and irregularly spaced in *pitx2c*$^{-/-}$ atria, and Z discs and M lines were poorly defined (Fig. 1 *R* and *T*). These data suggest that loss of Pitx2c leads to cardiomyopathy phenotypes in adult zebrafish.

Next, we performed electrocardiogram (ECG) analysis (Fig. 2) to assess cardiac electrophysiology. Cardiac arrhythmia was observed in ECG traces from *pitx2c*$^{+/-}$ and *pitx2c*$^{-/-}$ animals (Fig. 2 *B* and *C*) as well as prolonged RR intervals (the time between ventricular depolarizations) (Fig. 2*E*). We also observed a reduction in the average heart rate in both *pitx2c*$^{+/-}$ (93.3 ± 6.3 bpm) and *pitx2c*$^{-/-}$ (105.0 ± 7.9 bpm) fish compared to *pitx2c*$^{+/+}$ siblings (146.4 ± 7.2 bpm) (Fig. 2*D*). P-wave duration (Fig. 2*F*) and PR intervals (representing atrial depolarization) (Fig. 2*G*) were significantly increased in *pitx2c*$^{+/-}$ (51.33 ± 3.34 ms; 78.91 ± 3.62 ms, respectively) and *pitx2c*$^{-/-}$ (57.61 ± 4.83 ms; 87.13 ± 6.93 ms) fish compared with *pitx2c*$^{+/+}$ siblings (35.75 ± 2.43 ms; 59.30 ± 3.20 ms, respectively), indicating atrial conduction defects. In contrast, QT and QRS intervals, the time from ventricular contraction until relaxation and ventricular depolarization, respectively, were not significantly different between the genotypes (Fig. 2 *H* and *I*). Together, these data indicate that loss of Pitx2c leads to atrial conduction defects without affecting the ventricular conduction system.

Loss of Pitx2c Function Leads to Mitochondrial Defects in the Adult Heart. Cellular metabolic conditions are closely linked to the high-energy demand of the cardiac contractile machinery. Accordingly, altered cardiac energetics have been reported in human and experimental AF conditions (23, 24). The mitochondrial phenotypes observed by TEM (Fig. 1*P*) led us to hypothesize that cardiac

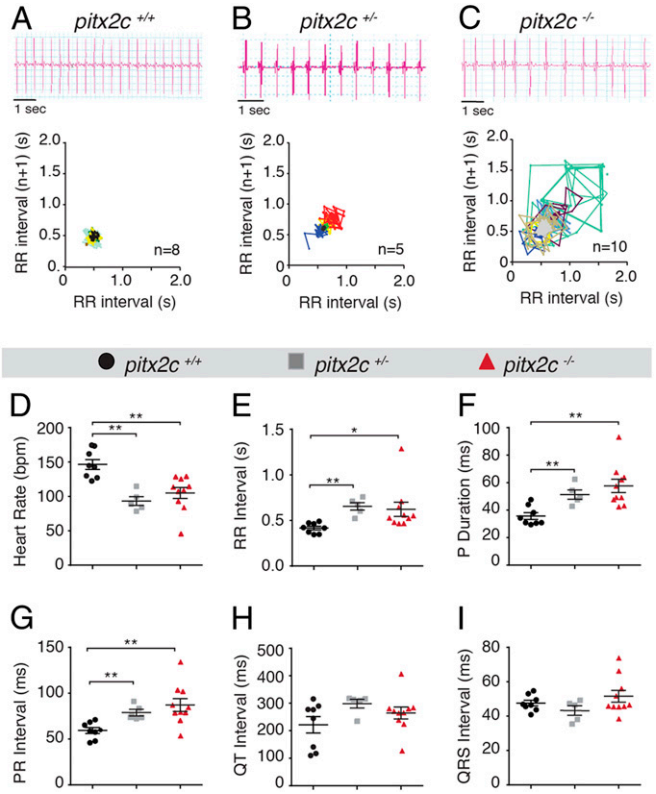

Fig. 2. Cardiac arrhythmia and prolonged atrial depolarization in *pitx2c*$^{-/-}$ adult hearts. Electrical conduction properties of 8-month postfertilization (mpf) adult hearts by ECG analysis. Representative ECG traces and Poincaré plots of consecutive RR intervals from *pitx2c*$^{+/+}$ (*A*), *pitx2c*$^{+/-}$ (*B*), and *pitx2c*$^{-/-}$ (*C*) hearts. Individual fish are each represented by a differently colored line. Quantification of heart rate (*D*), RR interval (*E*), P-wave duration (*F*), PR interval (*G*), QT interval (*H*), and QRS interval (*I*). *pitx2c*$^{+/-}$ and *pitx2c*$^{-/-}$ fish exhibit a variable and lower heart rate (*B*–*E*) and disrupted atrial conduction (*F* and *G*), while the ventricular conduction system seems unaffected (*H* and *I*). Error bars correspond to SEM. **P* < 0.05 by 1-way ANOVA; ***P* < 0.01 by 1-way ANOVA.

metabolism was compromised in *pitx2c*$^{-/-}$ hearts. To test this hypothesis, we measured mitochondrial respiration and reactive oxygen species (ROS) production. While overall respiration was slightly increased in *pitx2c*$^{-/-}$ atria (*SI Appendix*, Fig. S2), ROS/O_2 levels were lower in *pitx2c*$^{-/-}$ atria (0.004 ± 0.001 pmol H_2O_2/JO_2) compared with *pitx2c*$^{+/+}$ siblings (0.014 ± 0.012 pmol H_2O_2/JO_2) (*SI Appendix*, Fig. S2). In contrast, we observed reduced maximal mitochondrial respiration (Electron Transport System State 3) in *pitx2c*$^{-/-}$ ventricles (76.7 ± 14.5 pmol O_2) compared with *pitx2c*$^{+/+}$ siblings (98.7 ± 16.7 pmol O_2) (*SI Appendix*, Fig. S2), suggesting reduced oxidative phosphorylation capacity. To determine whether the alterations in respiration could result from changes in mitochondrial mass, we measured mitochondrial DNA (mtDNA) content in adult atria. mtDNA content was increased by ~30% in *pitx2c*$^{-/-}$ atria compared with *pitx2c*$^{+/+}$ siblings (Fig. 3*A*). These data are in line with the abnormal mitochondrial morphology observed in *pitx2c*$^{-/-}$ hearts (Fig. 1*P*), including the large mitochondrial clusters (Fig. 3*B*).

Direct Pitx2 target genes identified in neonatal mouse cardiac regeneration models include regulators of mitochondrial function, oxidation–reduction, and the respiratory chain (18, 25). To test whether these genes are regulated by Pitx2c in adult zebrafish hearts, we examined mRNA levels in atrial tissue by qPCR (Fig. 3*C*). We first examined the expression of the previously identified direct targets *hcn4* and *cox7c* (9, 18). As reported in

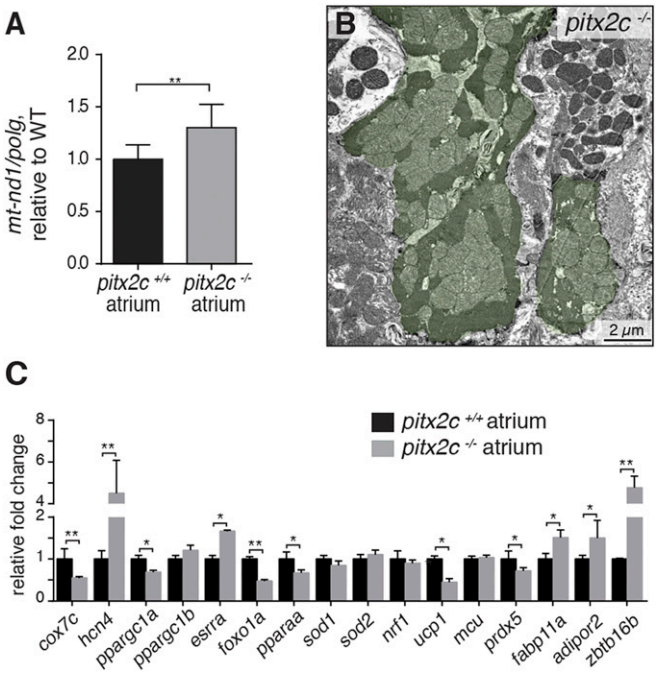

Fig. 3. Mitochondrial and metabolic changes in *pitx2c*$^{-/-}$ adult atria. (*A*) Quantification of relative mtDNA content in *pitx2c*$^{+/+}$ and *pitx2c*$^{-/-}$ atria by qPCR. (*B*) Representative image of mitochondrial clusters (highlighted in green) observed in *pitx2c*$^{-/-}$ adult hearts by TEM ($n = 3$). (*C*) qPCR of known PITX2 targets as well as additional metabolic genes in *pitx2c*$^{+/+}$ and *pitx2c*$^{-/-}$ adult atria. Significant down-regulation of *cox7c*, *ppargc1a*, *foxo1a*, *pparaa*, *ucp1*, and *prdx5* mRNA levels and up-regulation of *hcn4* and *esrra* as well as adipogenic genes *fabp11a*, *adipor2*, and *zbtb16b* mRNA levels are observed in *pitx2c*$^{-/-}$ atria (*C*). Error bars correspond to SEM. *$P < 0.05$ by unpaired *t* test; **$P < 0.01$ by unpaired *t* test.

mouse, we observed up-regulation of *hcn4* and down-regulation of *cox7c* in *pitx2c*$^{-/-}$ atria compared with *pitx2c*$^{+/+}$ siblings. We then screened a panel of genes involved in cellular metabolism. *pitx2c*$^{-/-}$ atria exhibited significant reduction in *ppargc1a*, *foxo1a*, *pparaa*, *ucp1*, and *prdx5* mRNA levels and up-regulation of *esrra*, *fabp11a*, *adipor2*, and *zbtb16b* mRNA levels (Fig. 3*C*). Together, these gene expression changes indicate alterations in oxidative phosphorylation and redox status of the heart as well as increased adipogenesis.

Pitx2c Controls Cardiac Rhythmicity in Zebrafish Larvae. One of the major questions surrounding AF initiation is whether changes to developmental genes can predispose to AF manifestation later in life. Therefore, we analyzed the phenotypic onset in *pitx2c*$^{-/-}$ animals by testing for cardiac arrhythmia during developmental stages. To this end, we performed high-speed spinning disc confocal imaging to record bright-field movies of beating larval hearts (Movies S3 and S4) and plotted kymographs to visualize and quantify cardiac intervals (Fig. 4 *A* and *B*). Larvae were scored as sinus rhythm (Fig. 4 *A* and *A′*) or arrhythmia (Fig. 4 *B* and *B′*) based on the absence or presence of irregular cardiac intervals, respectively. We found that a subset of *pitx2c*$^{-/-}$ larvae was arrhythmic starting at 120 h postfertilization (hpf), and phenotype penetrance increased with age (*SI Appendix*, Fig. S3). We then quantified heart rate variation in zebrafish larvae at 120 hpf by calculating the root mean square of the successive differences (RMSSD) of cardiac cycles, a method used to assess short-term heart rate variability in humans (26). As RMSSD measurements reflect beat-to-beat variability, elevated RMSSD values indicate arrhythmic events. Indeed, quantification of RMSSD indices revealed elevated beat-to-beat variability in *pitx2c*$^{-/-}$ larvae (95.77 ± 60.62 ms) compared with *pitx2c*$^{+/+}$ siblings (35.09 ± 20.90 ms) (Fig. 4*C*). Therefore, we conclude that loss of *pitx2c* leads to cardiac arrhythmia during early larval stages.

Developmental Changes in Sarcomeric and Metabolic Gene Expression Precede the Onset of Cardiac Arrhythmia. To explore molecular mechanisms prior to the onset of cardiac arrhythmia, we identified Pitx2c-dependent transcriptional changes by RNA sequencing (RNA-seq) of hearts isolated from 56-hpf *pitx2c*$^{+/+}$ and *pitx2c*$^{-/-}$ embryos. We selected this stage because *pitx2c* mRNA levels are higher than at 7 days postfertilization (27). In parallel, we profiled the transcriptome of hearts from a line in which *pitx2c* is overexpressed specifically in CMs: *Tg*(*myl7:pitx2c-P2A-H2BGFP*) (hereafter referred to as *pitx2c*^{GOF}) (*SI Appendix*, Fig. S4). Overexpression of *pitx2c* in CMs resulted in a dramatic increase in atrial CM number by 48 hpf; accordingly, this overgrowth led to defective cardiac morphogenesis and lethality at early larval stages (*SI Appendix*, Fig. S4*D*).

We identified 115 differentially expressed genes comparing *pitx2c*$^{+/+}$ with *pitx2c*$^{-/-}$ hearts and 393 differentially expressed genes comparing *pitx2c*$^{+/+}$ with *pitx2c*^{GOF} hearts (*SI Appendix*, Fig. S5*A*). Next, we performed pathway analyses based on gene expression differences comparing *pitx2c*$^{+/+}$ with *pitx2c*$^{-/-}$ or *pitx2c*^{GOF} hearts. Gene set enrichment analysis showed significant enrichment of Kyoto Encyclopedia of Genes and Genomes (KEGG) pathways for carbon metabolism, oxidative phosphorylation, and cardiac muscle contraction in both *pitx2c*$^{-/-}$ (*SI Appendix*, Fig. S5*B*) and *pitx2c*^{GOF} hearts (*SI Appendix*, Fig. S5*C*). Comparing these genes with a previously published Pitx2 chromatin immunoprecipitation sequencing (ChIP-seq) dataset (18) indicates that a proportion of the orthologous mouse genes have Pitx2 binding sites and thus, that at least some of the differentially expressed zebrafish genes might be direct Pitx2c targets (*SI Appendix*, Fig. S5*D*).

To validate the RNA-seq data, we performed qPCR on dissected hearts from 56-hpf *pitx2c*$^{+/+}$, *pitx2c*$^{-/-}$, and *pitx2c*^{GOF} embryos (*SI Appendix*, Fig. S6). Known PITX2 target genes *hcn4* and *jph2* (8) were significantly up-regulated in *pitx2c*$^{-/-}$ embryonic hearts. We also measured mRNA levels of selected genes encoding metabolic regulators and found significant down-regulation of *ppargc1a*, which is involved in oxidative metabolism (*SI Appendix*, Fig. S6). Similar to what has been reported in mouse (18), we observed up-regulation of the antioxidant gene *sod1* in zebrafish *pitx2c*^{GOF} hearts. Furthermore, several genes involved in the cytochrome oxidase complex or mitochondrial Complexes I and III were down-regulated in *pitx2c*$^{-/-}$ and *pitx2c*^{GOF} hearts. These data suggest that Pitx2c controls a set of genes that regulate the redox status of atrial CMs.

Next, we investigated whether the changes observed in mRNA levels in embryonic hearts were accompanied by sarcomere and metabolic defects. To examine sarcomere phenotypes, we analyzed 50-hpf *pitx2c*$^{-/-}$ embryos in the *Tg*(*myl7:LA-GFP*) background (Fig. 4 *D* and *E*). Subtle defects in sarcomere organization were visible by 50 hpf, prior to the stage when arrhythmia was observed. While sarcomeres in the *pitx2c*$^{+/+}$ hearts were clearly organized perpendicular to the direction of flow (Fig. 4*D*), sarcomeres in *pitx2c*$^{-/-}$ hearts appeared wavy and randomly positioned, with discontinuity across adjacent CMs (Fig. 4*E*). These observations were also confirmed by TEM analysis (Fig. 4 *F*–*I*).

To evaluate cardiac metabolism in larvae, we analyzed the mitochondrial redox state of 120-hpf *pitx2c*$^{-/-}$ hearts using a genetically encoded roGFP2 fluorescent probe (28) (Fig. 4 *J*–*L*). Quantification of the 405-/488-nm ratios from *pitx2c*$^{+/+}$, *pitx2c*$^{+/-}$, and *pitx2c*$^{-/-}$ hearts at 120 hpf were not significantly different between the genotypes (Fig. 4*L*). To test the effect of environmental stress, we delivered a 1-h heat shock (HS) at 37 °C to 120-hpf larvae just prior to imaging. HS induced significantly higher ROS levels in *pitx2c*$^{-/-}$ hearts (1.42 ± 0.06) compared with *pitx2c*$^{+/+}$ siblings (1.18 ± 0.04, $P = 0.008$), suggesting higher levels

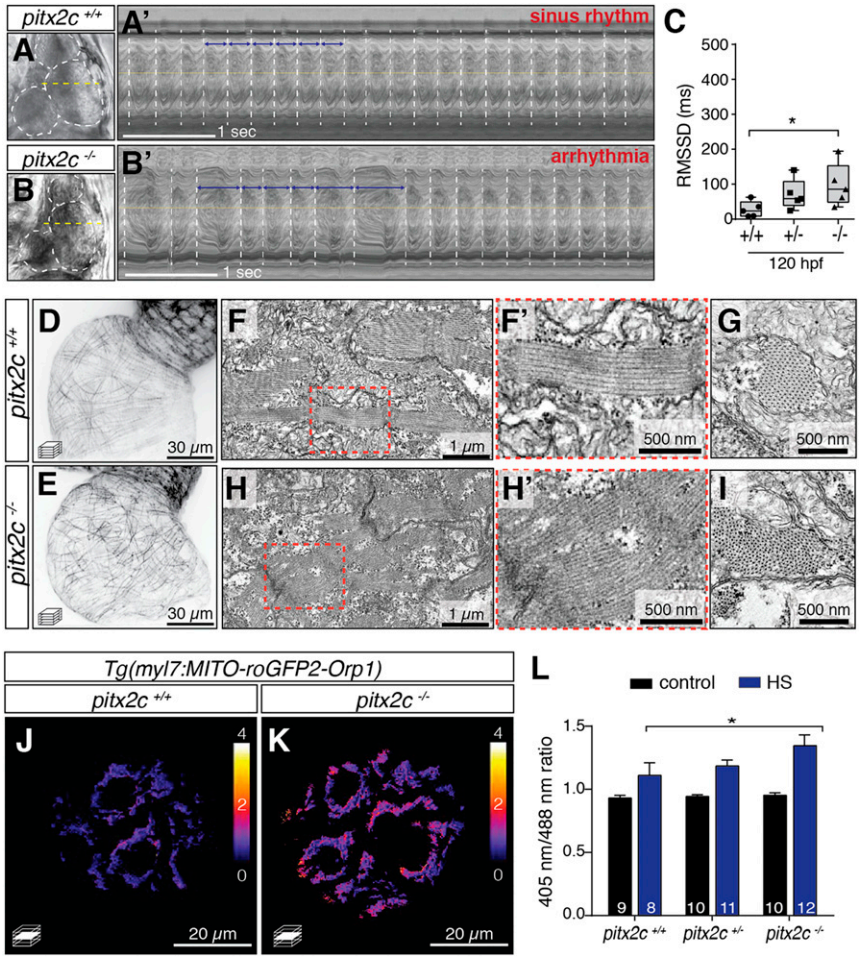

Fig. 4. Cardiac arrhythmia in *pitx2c*$^{-/-}$ larvae is preceded by sarcomere and metabolic defects. (*A*–*C*) Analysis of heart rate variability in larval zebrafish using high-speed imaging. Bright-field images of 120-hpf *pitx2c*$^{+/+}$ (*A*) and *pitx2c*$^{-/-}$ (*B*) hearts. Representative kymographs of sinus rhythm (*A′*) and arrhythmia (*B′*). White dashed lines mark each cardiac cycle; blue arrows denote the duration between consecutive contractions. Box-and-whisker plot of the RMSSD between consecutive cardiac cycles (*C*). Each data point represents the average interval calculated from 8 to 10 cardiac cycles of individual larvae. Increased variation is observed in *pitx2c*$^{-/-}$ larvae compared with *pitx2c*$^{+/+}$ siblings. Error bars correspond to SEM from at least 2 independent experiments. **P* < 0.05 by unpaired *t* test. (*D* and *E*) Confocal images of cardiac sarcomeres in 50-hpf *Tg(myl7:LA-EGFP); pitx2c*$^{+/+}$ (*D*) and *pitx2c*$^{-/-}$ (*E*) siblings. (*F*–*I*) TEM images of 56-hpf hearts ($n = 3$); higher magnification of the region outlined in red is shown in *F′* and *H′*. Embryonic sarcomeres appear wavy and less organized in *pitx2c*$^{-/-}$ compared with *pitx2c*$^{+/+}$. (*J*–*L*) Redox-state analysis of 120-hpf *pitx2c*$^{+/+}$ and *pitx2c*$^{-/-}$ atria expressing the *Tg(myl7:MITO-roGFP2-Orp1)* ROS biosensor. Calibration bar shows the relative 405-/488-nm ratio. (*L*) Quantification of 405-/488-nm ratios in control conditions or following a 1-h HS at 37 °C prior to imaging. Following HS, increased ROS levels were detected in all 3 genotypes; a stronger increase was observed in *pitx2c*$^{-/-}$ hearts, suggesting increased levels of oxidative stress compared with *pitx2c*$^{+/+}$ siblings (*L*). Error bars correspond to SEM from at least 2 independent experiments. **P* < 0.05 by unpaired *t* test.

of oxidative stress in the absence of Pitx2 function (Fig. 4*J*). Given that the induction of ROS levels on HS was higher in *pitx2c*$^{-/-}$ larvae, we wondered whether such environmental stress could exacerbate the cardiac arrhythmia phenotype. Indeed, HS significantly increased the proportion of *pitx2c*$^{-/-}$ arrhythmic larvae (from ∼25 to ∼60%) (Fig. 5*A*) and RMSSD intervals (Fig. 5*B*).

Metabolic Stress Is Required, but Not Sufficient, to Drive Cardiac Arrhythmia in Zebrafish Larvae. Transcriptional profiling and functional data suggest that both sarcomere and metabolic abnormalities are present in *pitx2c*$^{-/-}$ larvae prior to the onset of cardiac arrhythmia. Therefore, we next queried whether the contribution of these two factors could be separated. To test this possibility, embryos from *pitx2c*$^{+/-}$ incrosses were treated with 100 μM NAC, a potent ROS scavenger. Different treatment protocols were used to determine a precise temporal window of efficacy between 24 and 120 hpf. While HS did not induce cardiac arrhythmia in *pitx2c*$^{+/+}$ siblings, 60% of *pitx2c*$^{-/-}$ larvae were arrhythmic (Fig. 5*C*, HS alone), with significant beat-to-beat variability (157.2 ± 25.9 ms, $P = 0.017$) (Fig. 5*D*, HS alone). Continuous treatment with NAC from 24 to 120 hpf significantly decreased the proportion of *pitx2c*$^{-/-}$ larvae with cardiac arrhythmia to ∼25% (Fig. 5*C*) and reduced heart rate variability to 64.4 ± 12.3 ms ($P = 0.0014$) (Fig. 5*D*). These data suggest that increased ROS levels are an important driver of cardiac arrhythmia.

To investigate whether metabolic stress alone could trigger arrhythmia in the absence of sarcomere defects, we analyzed 2 models of metabolic insufficiency: Mia40a, an oxidoreductase essential for mitochondrial protein biogenesis (29, 30), and Ppargc1a, a master regulator of oxidative metabolism (31). In both models, we failed to observe a significant number of hearts that were arrhythmic, although HS did lead to more variability in cardiac intervals in both *mia40a*$^{-/-}$ (45.00 ± 10.64 and 56.08 ± 58.40 ms in control and HS, respectively) and *ppargc1a*$^{-/-}$ (22.60 ± 3.47 and 52.08 ± 38.52 ms in control and HS, respectively) compared with heterozygous and wild-type siblings (*SI Appendix*, Fig. S7). Taken together, these data suggest that metabolic

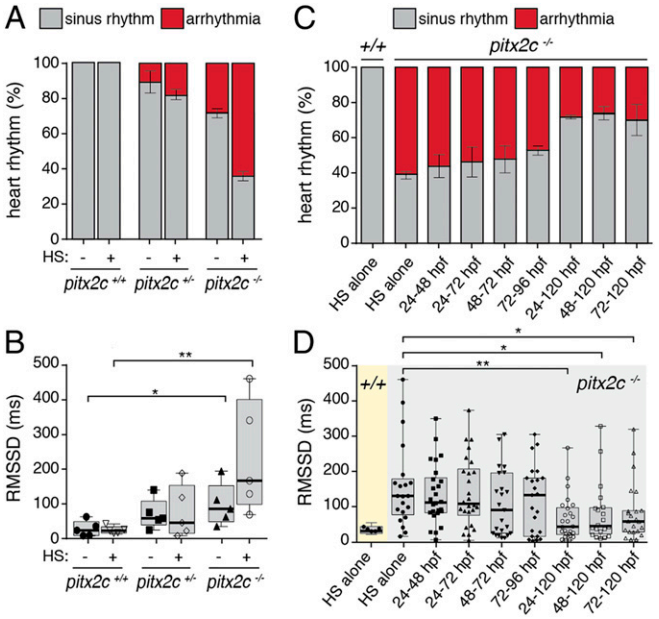

Fig. 5. Antioxidant treatment reduces the incidence of cardiac arrhythmia in *pitx2c*$^{-/-}$ larvae. (*A* and *B*) Effect of HS on the development of cardiac arrhythmia in 120-hpf larvae. HS (1 h at 37 °C) was performed ∼3 h prior to imaging. Proportion of larvae with sinus rhythm (gray) or arrhythmia (red; *A*). Box-and-whisker plots of RMSSD values in control conditions or following HS (*B*). Error bars indicate SEM from at least 2 independent experiments; $n > 10$ larvae per condition. (*C* and *D*) Treatment of larvae with 100 μM NAC at the indicated time points prior to HS and analysis of cardiac rhythm. Proportion of larvae with sinus rhythm (gray bars) or arrhythmia (red bars) following NAC treatment (*C*). Box-and-whisker plots of RMSSD values from *pitx2c*$^{+/+}$ (yellow) and *pitx2c*$^{-/-}$ (gray) in control conditions or following NAC treatment (*D*). Each data point represents the average interval calculated from 8 to 10 cardiac cycles of individual larvae. Treatment of *pitx2c*$^{-/-}$ larvae starting from 24, 48, or 72 to 120 hpf significantly reduced the number of arrhythmic hearts compared with HS alone (*D*). Error bars indicate SEM from at least 2 independent experiments. $n > 20$ *pitx2c*$^{-/-}$ animals per condition. $^{*}P < 0.05$ by unpaired *t* test; $^{**}P < 0.01$ by unpaired *t* test.

stress is necessary, but not sufficient, for the development of arrhythmias.

Discussion

Zebrafish offer unique advantages to study adult cardiac phenotypes. Compared with rodents, many aspects of zebrafish cardiac electrophysiology are more closely aligned with those of humans, including heart rate, developmental physiology, and cardiac action potential characteristics (32, 33). Indeed, modeling human arrhythmia in zebrafish has provided significant insight into mechanisms of conduction defects (33–36). Additionally, most dilated cardiomyopathy genes in humans have a corresponding ortholog in zebrafish (37), and zebrafish mutants in these genes reveal phenotypes resembling human cardiomyopathies (38, 39). Thus, from genetic, developmental, and electrophysiological perspectives, the zebrafish model is highly complementary to established in vivo models and may offer particular strengths over some of the existing models.

In this study, we describe the phenotypes observed in larval and adult zebrafish hearts following loss of Pitx2c function and propose that the *pitx2c* mutant can serve as a model of cardiac arrhythmia. We find atrial conduction defects, structural remodeling, and altered cardiac metabolism resembling the phenotypes observed in human AF patients. In comparison with rodent models of AF, *pitx2c*$^{-/-}$ zebrafish display an arrhythmia phenotype without pacing, thus representing an animal model of spontaneous arrhythmia. Furthermore, we detected cardiac phenotypes in a subset of adult *pitx2c*$^{+/-}$ zebrafish, similar to what is observed in *PITX2*$^{+/-}$ humans and mice (5).

Traditionally, AF has been primarily considered an electrophysiological disease. Indeed, Pitx2 has been shown to directly regulate targets, including ion channel genes, that modulate electrical conduction properties. Our RNA-seq analysis of both gain- and loss-of-function embryonic hearts revealed dysregulation of some of these targets, including *ryr2*, *cacna1g*, *jph2*, and *kcnq1* as well as *atp2a1* and *atp2a2*. These data indicate that Pitx2 regulates ion channel gene expression during cardiac development in zebrafish as has been shown in mouse (8, 9). We hypothesize that altered expression of ion channel genes (e.g., *hcn4*) in conjunction with sarcomere and metabolic defects in embryonic and adult hearts all contribute to the observed cardiac phenotypes.

In recent years, several reports have expanded our understanding of AF as a complex multifactorial disease. These studies suggest that mutations in genes that compromise sarcomere structure can also lead to AF phenotypes (19–21, 40). Our analyses of *pitx2c*$^{-/-}$ adult atria revealed significantly compromised cardiac tissue integrity by histology and TEM analysis as well as cardiac dysfunction by echocardiography. Additionally, we detected alterations in sarcomere organization in embryos long before extensive remodeling and electrophysiological defects are observed in adults. RNA-seq profiling of embryonic hearts also identified many differentially expressed genes associated with cardiac contraction. Many of these features are also observed in models of hypertrophic cardiomyopathy (41), and we, therefore, hypothesize that an underlying atrial cardiomyopathy precedes the development of arrhythmia, fibrosis, and other hallmarks of AF. These zebrafish data are in further support of the hypothesis that atrial cardiomyopathy predisposes the human heart to AF (19–21, 40).

Pitx2 activates a set of stress-response genes during skeletal muscle development (42) as well as during cardiac regeneration (18). Furthermore, Pitx2 is important for the maintenance of mitochondrial structure and function (25) and regulates the expression of mitochondrial genes in the mouse heart (18, 25). We found that some of these genes are similarly dysregulated in zebrafish embryonic hearts and observed increased ROS levels in *pitx2c*$^{-/-}$ larval hearts. As *Pitx2c* expression is enriched in the atria of zebrafish and mice, we hypothesize that it modulates the expression of metabolic genes in this chamber. We also observed in *pitx2c*$^{-/-}$ atria increased mtDNA content without a significant impact on mitochondrial respiratory capacity; this presumed increase in the number of mitochondria without a concomitant increase in respiration suggests a defect in mitochondrial function.

We observed that continuous NAC treatment reduced the proportion of arrhythmic *pitx2c*$^{-/-}$ larvae, indicating that increased ROS levels contribute to the development of the cardiac arrhythmia phenotype. However, we did not observe an arrhythmogenic phenotype in *mia40a* and *ppargc1a* models of metabolic insufficiency, suggesting that arrhythmias do not arise solely due to metabolic alterations. Altogether, these data indicate that metabolic stress is required, but not sufficient, for the development of cardiac arrhythmia in larvae. As HS treatment increased ROS levels more significantly in *pitx2c*$^{-/-}$ larval hearts compared with *pitx2c*$^{+/+}$, we hypothesize that *pitx2c* mutants are more sensitive than wild types to environmental stress, perhaps in part by a reduction in ROS scavengers. Therefore, increased ROS levels in conjunction with cardiac sarcomere defects contribute to the development of a cardiac arrhythmia phenotype in zebrafish larvae. It is also important to consider that several sarcomeric proteins are ROS sensitive. In many cases, redox modifications resulting in oxidation or nitrosylation can disrupt the function of such proteins and contribute to contractile dysfunction (43–45). This aspect of cross-talk between sarcomere and metabolic defects may also be highly relevant in the *pitx2c* model of cardiac arrhythmia.

Altogether, our data support the hypothesis that sarcomere defects in conjunction with metabolic stress are required for the development of electrical dysfunction and other hallmarks of AF. We propose a model whereby sarcomere and metabolic defects are present in the *pitx2c*$^{-/-}$ embryonic heart, and they act as arrhythmogenic substrates already at these early stages of development (*SI Appendix*, Fig. S8). With age and continued cardiac stress, phenotypes such as atrial conduction defects and structural remodeling are observed. We hypothesize that atrial energetics attempt to compensate by increased mitochondrial respiration, which may consequently lead to oxidative stress. At late adult stages, many of the phenotypes observed in *pitx2c*$^{-/-}$ hearts are suggestive of heart failure, recapitulating the proposed end point diagnosis of some untreated AF patients. In summary, we propose that the pathogenesis of arrhythmia and AF-like phenotypes can be driven by early sarcomere and metabolic changes that lead to atrial myopathy and altered atrial cardiac energetics.

Materials and Methods

Detailed methods can be found in *SI Appendix*.

Zebrafish Husbandry. Zebrafish husbandry was performed under standard conditions in accordance with the European Convention for the Protection of Vertebrate Animals Used for Experimental and Other Scientific Purposes. Procedures involving animals were approved by the veterinary department of the Regional Board of Darmstadt and the Danish Animal Experimental board (personal project license 2017-15-0201-01305).

ECG Analysis. Adult zebrafish were anesthetized in 0.03% Tricaine/MS-222 (Sigma-Aldrich) in fish tank water, and the zebrafish were placed dorsal side down in a damp sponge. ECG traces were analyzed beat per beat using a minimum of 30 consecutive beats.

RNA-seq. Detailed methods can be found in *SI Appendix*. RNA-seq datasets have been deposited to the Gene Expression Omnibus repository under accession number GSE128511.

Data Analysis. Images were analyzed using ImageJ/FIJI and Zen software (Zeiss). Statistical analyses were performed using Prism (GraphPad).

Data Availability Statement. All data discussed in the paper are available to readers in the Gene Expression Omnibus repository under accession number GSE128511.

ACKNOWLEDGMENTS. We thank M. Santoro and E. Panieri for the *Tg(myl7:MITO-roGFP2-Sce.Hyr1)*^{uto54Tg} line and imaging advice; J. Martin and M. Zhang for sharing the *Pitx2* datasets; H. Schultheis and M. Looso for bioinformatics support; B. Berge for TEM assistance; S. Allanki for sharing reagents; S. Howard, B. Grohmann, M. Ploch, P. Neeb, and C. Kremser for technical support; and members of the laboratory of D.Y.R.S. for fruitful discussions. This work was supported by funds from the Deutsches Zentrum für Herz-Kreislauf-Forschung (German Centre for Cardiovascular Research, to M.M.C.), the Novo Nordisk Foundation (to M.S.O. and P.R.L.), the John and Birthe Meyer Foundation (to M.S.O. and P.R.L.), the Deutsche Forschungsgemeinschaft (project no. 394046768 SFB1366/project A4) (to R.M.-J. and D.Y.R.S.), and the Max Planck Society and Leducq Foundation (to D.Y.R.S.).

1. D. F. Gudbjartsson *et al.*, Variants conferring risk of atrial fibrillation on chromosome 4q25. *Nature* **448**, 353–357 (2007).
2. P. T. Ellinor *et al.*, Meta-analysis identifies six new susceptibility loci for atrial fibrillation. *Nat. Genet.* **44**, 670–675 (2012).
3. S. A. Lubitz *et al.*, Novel genetic markers associate with atrial fibrillation risk in Europeans and Japanese. *J. Am. Coll. Cardiol.* **63**, 1200–1210 (2014).
4. C. Roselli *et al.*, Multi-ethnic genome-wide association study for atrial fibrillation. *Nat. Genet.* **50**, 1225–1233 (2018).
5. J. Wang *et al.*, Pitx2 prevents susceptibility to atrial arrhythmias by inhibiting left-sided pacemaker specification. *Proc. Natl. Acad. Sci. U.S.A.* **107**, 9753–9758 (2010).
6. P. Kirchhof *et al.*, PITX2c is expressed in the adult left atrium, and reducing Pitx2c expression promotes atrial fibrillation inducibility and complex changes in gene expression. *Circ. Cardiovasc. Genet.* **4**, 123–133 (2011).
7. G. Ammirabile *et al.*, Pitx2 confers left morphological, molecular, and functional identity to the sinus venosus myocardium. *Cardiovasc. Res.* **93**, 291–301 (2012).
8. Y. Tao *et al.*, Pitx2, an atrial fibrillation predisposition gene, directly regulates ion transport and intercalated disc genes. *Circ. Cardiovasc. Genet.* **7**, 23–32 (2014).
9. R. D. Nadadur *et al.*, Pitx2 modulates a Tbx5-dependent gene regulatory network to maintain atrial rhythm. *Sci. Transl. Med.* **8**, 354ra115 (2016).
10. E. Lozano-Velasco *et al.*, Pitx2 impairs calcium handling in a dose-dependent manner by modulating Wnt signalling. *Cardiovasc. Res.* **109**, 55–66 (2016).
11. L. A. Aguirre *et al.*, Long-range regulatory interactions at the 4q25 atrial fibrillation risk locus involve PITX2c and ENPEP. *BMC Biol.* **13**, 26 (2015).
12. A. Chinchilla *et al.*, PITX2 insufficiency leads to atrial electrical and structural remodeling linked to arrhythmogenesis. *Circ. Cardiovasc. Genet.* **4**, 269–279 (2011).
13. C. Mora *et al.*, Generation of induced pluripotent stem cells (iPSC) from an atrial fibrillation patient carrying a PITX2 p.M200V mutation. *Stem Cell Res.* **24**, 8–11 (2017).
14. A. Mechakra *et al.*, A novel PITX2c gain-of-function mutation, p.Met207Val, in patients with familial atrial fibrillation. *Am. J. Cardiol.* **123**, 787–793 (2019).
15. A. K. Ryan *et al.*, Pitx2 determines left-right asymmetry of internal organs in vertebrates. *Nature* **394**, 545–551 (1998).
16. M. E. Piedra, J. M. Icardo, M. Albajar, J. C. Rodriguez-Rey, M. A. Ros, Pitx2 participates in the late phase of the pathway controlling left-right asymmetry. *Cell* **94**, 319–324 (1998).
17. M. Logan, S. M. Pagan-Westphal, D. M. Smith, L. Paganessi, C. J. Tabin, The transcription factor Pitx2 mediates situs-specific morphogenesis in response to left-right asymmetric signals. *Cell* **94**, 307–317 (1998).
18. G. Tao *et al.*, Pitx2 promotes heart repair by activating the antioxidant response after cardiac injury. *Nature* **534**, 119–123 (2016).
19. N. Orr *et al.*, A mutation in the atrial-specific myosin light chain gene (MYL4) causes familial atrial fibrillation. *Nat. Commun.* **7**, 11303 (2016).
20. D. F. Gudbjartsson *et al.*, A frameshift deletion in the sarcomere gene MYL4 causes early-onset familial atrial fibrillation. *Eur. Heart J.* **38**, 27–34 (2017).
21. G. Ahlberg *et al.*, Rare truncating variants in the sarcomeric protein titin associate with familial and early-onset atrial fibrillation. *Nat. Commun.* **9**, 4316 (2018).
22. M. M. Collins *et al.*, Pitx2c orchestrates embryonic axis extension via mesendodermal cell migration. *eLife* **7**, e34880 (2018).
23. P. Korantzopoulos, T. M. Kolettis, D. Galaris, J. A. Goudevenos, The role of oxidative stress in the pathogenesis and perpetuation of atrial fibrillation. *Int. J. Cardiol.* **115**, 135–143 (2007).
24. C. X. Huang, Y. Liu, W. F. Xia, Y. H. Tang, H. Huang, Oxidative stress: A possible pathogenesis of atrial fibrillation. *Med. Hypotheses* **72**, 466–467 (2009).
25. L. Li *et al.*, *Pitx2* maintains mitochondrial function during regeneration to prevent myocardial fat deposition. *Development* **145**, dev168609 (2018).
26. F. Shaffer, J. P. Ginsberg, An overview of heart rate variability metrics and norms. *Front. Public Health* **5**, 258 (2017).
27. F. Gunawan *et al.*, Focal adhesions are essential to drive zebrafish heart valve morphogenesis. *J. Cell Biol.* **218**, 1039–1054 (2019).
28. E. Panieri, C. Millia, M. M. Santoro, Real-time quantification of subcellular H_2O_2 and glutathione redox potential in living cardiovascular tissues. *Free Radic. Biol. Med.* **109**, 189–200 (2017).
29. A. M. Sokol *et al.*, Loss of the Mia40a oxidoreductase leads to hepato-pancreatic insufficiency in zebrafish. *PLoS Genet.* **14**, e1007743 (2018).
30. A. Chacinska *et al.*, Essential role of Mia40 in import and assembly of mitochondrial intermembrane space proteins. *EMBO J.* **23**, 3735–3746 (2004).
31. J. J. Lehman *et al.*, Peroxisome proliferator-activated receptor gamma coactivator-1 promotes cardiac mitochondrial biogenesis. *J. Clin. Invest.* **106**, 847–856 (2000).
32. U. Ravens, Ionic basis of cardiac electrophysiology in zebrafish compared to human hearts. *Prog. Biophys. Mol. Biol.* **138**, 38–44 (2018).
33. D. J. Milan, C. A. Macrae, Zebrafish genetic models for arrhythmia. *Prog. Biophys. Mol. Biol.* **98**, 301–308 (2008).
34. N. C. Chi *et al.*, Genetic and physiologic dissection of the vertebrate cardiac conduction system. *PLoS Biol.* **6**, e109 (2008).
35. A. M. Ebert *et al.*, Calcium extrusion is critical for cardiac morphogenesis and rhythm in embryonic zebrafish hearts. *Proc. Natl. Acad. Sci. U.S.A.* **102**, 17705–17710 (2005).
36. R. Arnaout *et al.*, Zebrafish model for human long QT syndrome. *Proc. Natl. Acad. Sci. U.S.A.* **104**, 11316–11321 (2007).
37. Y. H. Shih *et al.*, Cardiac transcriptome and dilated cardiomyopathy genes in zebrafish. *Circ. Cardiovasc. Genet.* **8**, 261–269 (2015).
38. J. Bakkers, Zebrafish as a model to study cardiac development and human cardiac disease. *Cardiovasc. Res.* **91**, 279–288 (2011).
39. P. Gut, S. Reischauer, D. Y. R. Stainier, R. Arnaout, Little fish, big data: Zebrafish as a model for cardiovascular and metabolic disease. *Physiol. Rev.* **97**, 889–938 (2017).
40. S. H. Choi *et al.*; DiscovEHR study and the NHLBI Trans-Omics for Precision Medicine (TOPMed) Consortium, Association between titin loss-of-function variants and early-onset atrial fibrillation. *J. Am. Med. Assoc.* **320**, 2354–2364 (2018).
41. A. V. Dvornikov, P. P. de Tombe, X. Xu, Phenotyping cardiomyopathy in adult zebrafish. *Prog. Biophys. Mol. Biol.* **138**, 116–125 (2018).
42. A. L'honoré *et al.*, Redox regulation by Pitx2 and Pitx3 is critical for fetal myogenesis. *Dev. Cell* **29**, 392–405 (2014).
43. A. Janué, M. A. Odena, E. Oliveira, M. Olivé, I. Ferrer, Desmin is oxidized and nitrated in affected muscles in myotilinopathies and desminopathies. *J. Neuropathol. Exp. Neurol.* **66**, 711–723 (2007).
44. A. Grützner *et al.*, Modulation of titin-based stiffness by disulfide bonding in the cardiac titin N2-B unique sequence. *Biophys. J.* **97**, 825–834 (2009).
45. S. F. Steinberg, Oxidative stress and sarcomeric proteins. *Circ. Res.* **112**, 393–405 (2013).